# The THEMIS Array of Ground-based Observatories for the Study of Auroral Substorms

**S.B. Mende · S.E. Harris · H.U. Frey · V. Angelopoulos ·
C.T. Russell · E. Donovan · B. Jackel · M. Greffen ·
L.M. Peticolas**

**Abstract** The NASA Time History of Events and Macroscale Interactions during Substorms (THEMIS) project is intended to investigate magnetospheric substorm phenomena, which are the manifestations of a basic instability of the magnetosphere and a dominant mechanism of plasma transport and explosive energy release. The major controversy in substorm science is the uncertainty as to whether the instability is initiated near the Earth, or in the more distant >20 Re magnetic tail. THEMIS will discriminate between the two possibilities by using five in-situ satellites and ground-based all-sky imagers and magnetometers, and inferring the propagation direction by timing the observation of the substorm initiation at multiple locations in the magnetosphere. An array of stations, consisting of 20 all-sky imagers (ASIs) and 30-plus magnetometers, has been developed and deployed in the North American continent, from Alaska to Labrador, for the broad coverage of the nightside magnetosphere. Each ground-based observatory (GBO) contains a white light imager that takes auroral images at a 3-second repetition rate ("cadence") and a magnetometer that records the 3 axis variation of the magnetic field at 2 Hz frequency. The stations return compressed images, "thumbnails," to two central databases: one located at UC Berkeley and the other at the University of Calgary, Canada. The full images are recorded at each station on hard drives, and these devices are physically returned to the two data centers for data copying. All data are made available for public use by scientists in "browse products," accessible by using internet browsers or in the form of downloadable CDF data files (the "browse products" are described in detail in a later section). Twenty all-sky imager stations are installed and running at the time of this publication. An example of a substorm was observed on the 23rd of December 2006, and from the THEMIS GBO data, we found that the substorm onset brightening of the equatorward arc was a gradual process (>27 seconds), with minimal

S.B. Mende (✉) · S.E. Harris · H.U. Frey · V. Angelopoulos · L.M. Peticolas
Space Science Laboratory, University of California, Berkeley, CA 94720, USA
e-mail: mende@ssl.berkeley.edu

E. Donovan · B. Jackel · M. Greffen
University of Calgary, Calgary, Canada

V. Angelopoulos · C.T. Russell
University of California, Los Angeles, CA 90095, USA

morphology changes until the arc breaks up. The breakup was timed to the nearest frame (<3 s) and located to the nearest latitude degree at about $\pm 3^{\circ}$E in longitude. The data also showed that a similar breakup occurred in Alaska ~10 minutes later, highlighting the need for an array to distinguish prime onset.

## 1 Introduction

The NASA Time History of Events and Macroscale Interactions during Substorms (THEMIS) project is intended to answer fundamental questions regarding magnetospheric substorms (Angelopoulos 2008). THEMIS will distinguish between the two most likely magnetotail processes responsible for initiating substorms—local disruption of the near-tail plasma sheet current at <10 Re, or magnetic interaction with the rapid influx of plasma ejected from lobe flux annihilation at >20 Re (Lui 1991; Baker et al. 1996). Correlative observations from five identical probes located at strategic positions will document the phenomena and the timing of their occurrences, and will infer the direction of propagation of energy in the substorm process. If the process were to initiate with local current disruption at <10 Re, then the phenomena would be expected to propagate outward along the tail. Whereas if the initiation point were at the tail reconnection region at >20 Re, then the phenomena would be expected to propagate inward towards the earth and precede the auroral signature that is visible from the ground. It is therefore crucial to locate and time the onset of the auroral signature at substorm onset. The five identical probes (satellites) measure particles and fields on orbits which permit the alignment of the satellites in the tail while North America is in the night side. The satellite observations can be supplemented by a set of ground observatories in North America which will time the auroral breakup onset. There are three inner probes at ~10 Re that monitor current disruption onset, while two outer probes, one at 20 and one at 30 Re, monitor plasma acceleration due to magnetic reconfiguration, such as tail flux dissipation and/or field dipolarization. THEMIS answers many critical questions in radiation belt physics and solar wind-magnetosphere energy coupling, in addition to addressing its primary objective. Detailed design of the THEMIS mission, the satellites, and their instrumentation is described in accompanying articles. This paper will discuss the requirements that led to the design of the Ground Based Observatories, describe the instruments, the array concept and the analysis techniques, as well as data formats and data products. The technical implementation and deployment of the GBOs are discussed by Harris et al. (2008).

Magnetospheric substorms are impulsive changes in the energy balance of the magnetosphere. They were discovered during studies of auroral images taken from an array of simultaneously operating ground-based all-sky cameras (ASCAs) (Akasofu 1977). Substorms are highly evident in optical auroral observations as a sudden dynamic activity and brightening in a pre-existent quasi-steady arc structure, and subsequent rapid poleward and local time propagation of the auroral brightening. During the International Geophysical Year (IGY: July, 1957 to December 31, 1958) and the following International Geophysical Collaborations (the year 1959), auroral observations greatly improved. Globally, there were about 120 all-sky cameras, divided between the Northern and Southern Hemispheres in the approximate ratio of 3:1, but never more than half of the Arctic polar sky was under observation at any one time; this was due to land and sea distribution, and clouds (Akasofu 1963). During

the IGY, ASCA photographs were taken at most stations at 1-minute intervals during dark periods in fine weather; the exposure was 55 seconds followed by a 5-second period to move the film. The program produced a great volume of records, which has shed much insight into the morphology of a typical auroral substorm (Akasofu 1964, 1965, 1968; Davis 1966).

Since the IGY, several other attempts were made at fielding all-sky imagers and related instruments to study magnetospheric substorms. Magnetospheric substorms are a global phenomenon, therefore a single all-sky camera station is inadequate to study them. For this reason, several attempts have been made to field and operate chains of coordinated optical observatories. More recent ground-based arrays were/are the Canopus/Norstar array in Canada (Donovan et al. 2003), the United States AGO network in Antarctica (Mende et al. 1999; Rosenberg 2000) and the Magnetometers–Ionospheric Radars–All-sky Cameras Large Experiment (MIRACLE) network (Syrjäsuo et al. 2002) in Northern Fennoscandia and Svalbard for monitoring auroral ionospheric dynamics. The MIRACLE includes five newly implemented digital all-sky cameras of the type used in the THEMIS GBOs.

High-altitude satellite-based imaging has been the most productive way of documenting substorms on a global scale and for time periods relevant to substorm phases—substorms generally last from one to several hours. To make useful observations, satellites must have orbits that permit continuous observation for long periods of time. Thus low-altitude earth orbit (LEO) satellites are fundamentally unsuited for observations of substorm phases. DE-1 was the first high-altitude satellite that permitted extended duration of global auroral viewing (Frank et al. 1981; Frank and Craven 1988). The far ultraviolet wavelength band is strongly favored for space-based observations because it permits observation of the aurora in daytime sunlit conditions. Most importantly, no special effort is required to extend the dynamic range of the instrument to accommodate the relatively faint aurora in the presence of bright sunlit earth in the field-of-view. Thus many authors successfully pursued space-based substorm studies by using the ultraviolet imagers on POLAR (Torr et al. 1995) and IMAGE

2000/10/24
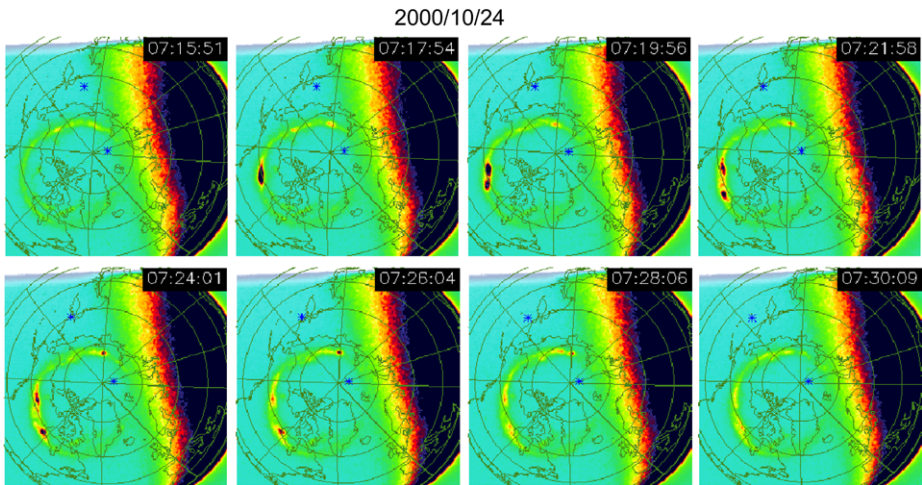


**Fig. 2** Global imaging of substorms. Substorm observed on the 24th of October 2000 by the Wideband Imaging Camera (WIC) on the NASA IMAGE satellite. Substorm onset occurred between 07:15:51 and 07:17:54. Although each exposure is only a 10-second integration, the 2 minute rotation period of the IMAGE satellite restricted the time resolution to about 2 minutes. THEMIS ground-based observatories need to make quasi-global images at a much higher repetition rate

(Mende et al. 2000) (Fig. 2). These latter instruments had adequate wavelength resolution to distinguish between auroras caused by low- and by high-energy electrons. In addition, the IMAGE FUV instrument had sufficient high spectral resolution to sense Doppler-shifted auroral hydrogen emission and distinguish proton-induced aurora from the optically thick and greatly intense geocorona.

It would have been very difficult to coordinate the orbit of a separate high-altitude and high-inclination imaging satellite to that of the five THEMIS spacecrafts, and cover the relevant part of the polar regions conjugate to the THEMIS satellites. A 63-degree inclination orbit satellite in a 12-hour orbit could have been synchronized to observe the northern Canadian arctic in the winter at midnight—however, such an arrangement would require launching a separate satellite platform into a specific orbit and would have been prohibitively expensive. It was decided early in the program that a GBO network would be a more cost-effective way of satisfying the needs of THEMIS to determine substorm onset location and timing. An additional drawback to high-altitude space-based imaging is the limitation on spatial resolution. It is difficult to satisfy the competing technical requirements arising from the need for global coverage and fine spatial resolution with a single space-based imager.

Substorm onsets can be determined from their characteristic magnetic signatures. A large westward Hall current is initiated at substorm onset, and magnetometers located near the onset point pick up the magnetic field change due to the ionospheric and magnetospheric currents overhead. Figure 3, upper box, illustrates the signature of a substorm onset taken with the GBO magnetometer located in Athabasca. The overhead westward current produces a "negative bay" as observed in the BH (magnetic north-south) component. The strong negative bay in the $B_z$ (vertical) component signifies that the bulk of the current was flowing northward of the station and the latitude of the onset was most probably located poleward of Athabasca. The two lower panels show a magnified view of the magnetic signature of a typical onset and recovery of a substorm.
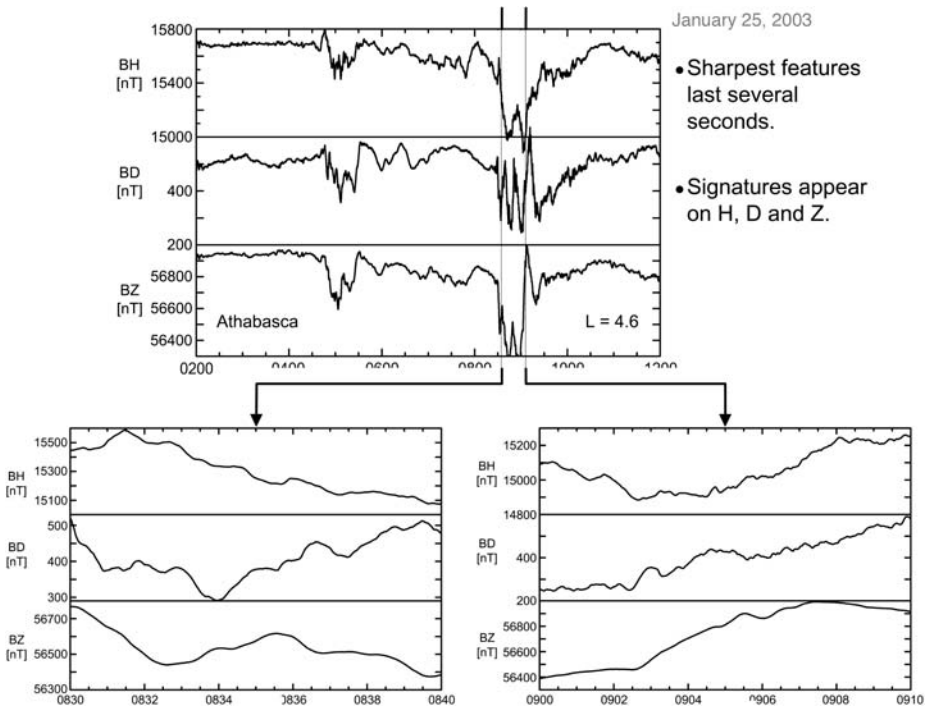
**Fig. 3** Magnetometer data illustrating typical substorm signatures

## 2 Requirement Definition

The primary, Level 1 THEMIS mission requirement is to be able to determine the time and location of the initial auroral intensification in magnetic local time (MLT) and latitude coordinates. This requirement is met with an array of all-sky imagers and ground magnetometers distributed over an 8-h geographic local time sector in northern Canada and Alaska. There are two ground magnetometers (GMAG) and at least one auroral zone ASI per MLT hour. The ASIs have a time resolution of $<10$ s and a spatial resolution $<1°$ of latitude.

Figure 4 shows substorm onset locations as observed by the IMAGE FUV experiment, with the originally proposed fields of views of 20 ASIs shown (Frey et al. 2004). The coverage of the all-sky imaging array would have been sufficient to capture the greatest majority of substorm onsets (asterisks), had all the GBOs been up and working at the time IMAGE was taking the data. It also shows that station coverage is quite comprehensive in latitude and that it covers a longitude region from 190 to approximately 310 degrees (east longitude). This is equivalent to local time coverage of 8 hours. Extensive coverage is desirable to cover substorms in which the onset occurs at various local times and latitudes.

The latitude resolution requirement of one degree of latitude is equivalent to a dipole $L$ value change $\Delta L$ of 0.2 at 60 degrees. From Fig. 4, it can be seen that substorm onset locations are seldom higher than 70 degrees magnetic. Thus the one degree of latitude resolution translates to $\Delta L = 1$, which is approximately equivalent to 1 Re distance in the near tail region.

With regard to time resolution, THEMIS needs to determine the substorm onset time corresponding to the time it takes for the plasma effects to propagate about 1 Re in the near
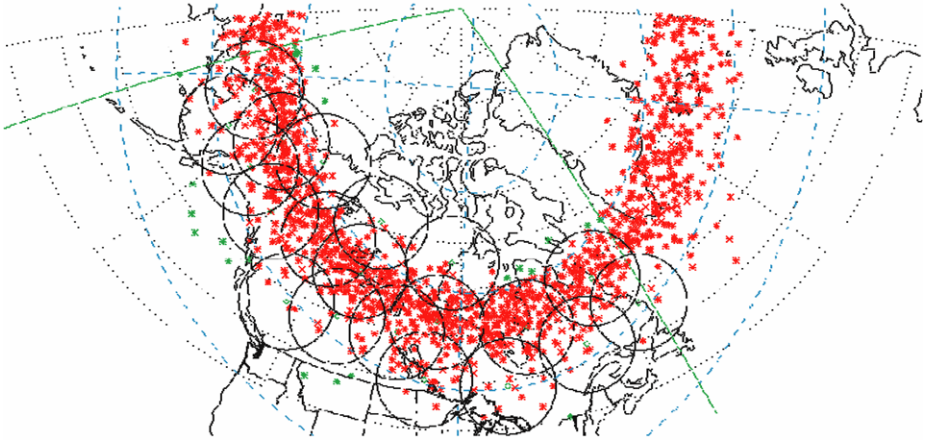
**Fig. 4** Substorm onset occurrences as observed by the IMAGE FUV experiment (*asterisks*) and the coverage of the THEMIS GBO stations

equatorial magnetosphere. The propagation speed is the Alfven speed,

$$V_a = B/(4\pi nm)^{1/2}.$$

In the equatorial region where the onsets occur the magnetic field $B$, is of the order of $\sim 50$ nT ($5 \times 10^{-4}$ gauss) or less. If we assume a lower limit of 1 particle per cm$^3$ of hydrogen ($m = 1.67240 \times 10^{-24}$ g) for the plasma density, the largest Alfven speed is $V_a = 1.09 \times 10^3$ km s. Thus one $L$ value propagation takes about 6 s and the substorm phenomena travel from regions >20 Re to <10 Re, taking about a minute. The waves would travel more slowly in weaker magnetic fields or in the presence of greater plasma densities. The THEMIS requirement of timing accuracy is 10 seconds. The practical limit of our hardware is an exposure cadence of 3 seconds, which satisfies the THEMIS time resolution requirement and provides definitive determination of substorm onset time.

A sample rate of 2 Hz was specified for the GMAG instrument to take advantage of the accurate timing and location of substorm onsets from Pi1 pulsations (1–40 s period). These pulsations are expected to provide more precise timing than the more widely-used Pi2 pulsations (40–150 s period) (Posch et al. 2004).

The coverage of a single ASI is approximately circular in geographic space, with a radial distance equivalent to about 4.5 degrees of latitude. At high latitudes (60 and above) this is equal to about twice as many degrees in longitude; thus each station is providing between 16 and 20 degrees of longitude, i.e., larger than 15 degree = 1 hour local time coverage (see Fig. 4). Therefore, 1 hour local time per ASI is adequate for contiguous coverage.

Using similar arguments, it can be shown that two GMAG instrument per one hour local time spacing provides sufficient resolution to determine the location of onset of the substorm current.

Substorm auroras are relatively bright. A threshold sensitivity of 10 kR would be quite adequate to satisfy THEMIS Level 1 requirements. As we will see, THEMIS ASIs have more than an order of magnitude higher sensitivity. Similarly, the detection of magnetic bays associated with substorms do not require very high sensitivity—1 nT sensitivity would be satisfactory. This is surpassed by the THEMIS GMAGs, whose sensitivity is in the 0.1 nT range.

In summary, the THEMIS GBOs are monitoring the auroral light and ionospheric currents across the North American continent in order to record the time, location, and evolution of the auroral signatures of substorms.

In Table 1, we have summarized the requirements of the GBO stations.

## 3 Observatory Chain Design

The most difficult THEMIS requirement demands comprehensive coverage of the North American sector of the auroral oval. In order to satisfy this requirement, 20 stations were needed. The station locations are given in Table 2. Figure 5 illustrates the station locations, with circles representing the fields-of-view of the all-sky cameras when taking a 160-degree total field projected to 110 km altitude. The diameter of each circle is about 9 latitude degrees. The station array provides fairly complete coverage, with the exception of a small gap between stations GILL–FSMI, GILL–KAPU and SNKQ–GBAY. Even with these small "holes," the system fulfills the THEMIS requirements. It is estimated that the array will cover over 90% of substorms occurring in the North American local time sector (Fig. 4).

When locating the stations it was necessary to consider the resource requirements at each prospective site. The stations require clear, unobstructed field of view (without lights), power, internet connection and some minimal custodian attention. Historically, it has been difficult to find sites that have power but only minimal exterior lighting. Large cities or population centers are generally unsuitable, due to light pollution. The requirement for quick data retrieval and "real time" programming/commanding capability demanded a high speed internet connection, further restricting the choices. Fortunately there are geosynchronous satellite-based internet providers and their service can be accessed even from the higher latitude stations. They can provide sufficient baud rates to allow the retrieval of the compressed Near Real Time (NRT) thumbnail ASI data, and full resolution GMAG data.

The technique for observing the global aurora from an array of stations is limited by the inherent distortion of the observing geometry, as illustrated in Fig. 6. For equal areas on the "sky" at auroral altitudes ($\sim$110 km) represented by $dx$, the corresponding angular distance $d\theta$ for a ground observer is compressed near the horizons, with increasing distance from the station. Conversely, outer pixels in the circular image represent larger regions of auroral precipitation than pixels near the middle.

Figures 7a and b illustrates an image from Rankin Inlet. Figure 7a represents the original image as it is read out and digitized from the CCD. A rayed arc is seen on the right half of the image and a thin, long east-west extended arc is seen near the bottom, in the vicinity of the horizon. Lights from a nearby settlement can be seen at the very bottom right of the image. The crosses represent the magnetically projected track of the NASA FAST auroral satellite that was passing through the field of view. Figure 7b is a representation of the same all-sky image projected on an imaginary layer at 110 km altitude. The distortions produced by this treatment are quite evident—the regions near the horizons are greatly extended. The method to create this image is called "backward projection" because this picture was produced by starting from the final latitude/longitude pixel matrix. This matrix represents the "bins" on the sky at an assumed 110 km altitude. These bins on the final image matrix are mapped to the appropriate pixels in the all-sky camera image. The pixel intensity in the all sky image pixel is simply copied as the output intensity in the latitude/longitude bin. This method is very simple and it overcomes the complexities of the mismatch in the area between the pixels in the all sky camera image and the corresponding latitude/longitude bins. In cases when the latitude/longitude bins spans multiple pixels in the all-sky camera

**Table 1** GBO requirement summary

| | Requirement driver | Requirement | Unit |
|---|---|---|---|
| | | **Imager** | |
| Field of view | Large spatial coverage 9 lat deg. circular | 170 | ° full angle |
| Spectral passband | Capture visible aurora | 400–700 (with IR filter) | nm |
| Sensitivity | Record substorm aurora | <1 (@ 5:1 S/N) | kR |
| Spatial resolution number of pixels | Locate substorm 1° of latitude (~100 km) | 32 (diameter all-sky-image) | pixel |
| Exposure duration | High cadence/ high sensitivity | Programmable, 1 | s |
| Cadence | Resolve substorm onset with 10 s accuracy | 3 | s |
| | | **Fluxgate magnetometer** | |
| Dynamic range | Cover the earth background field | ±72,000@0.01 nT resolution (~23 bits) | nT |
| DAC offset system | | 256 | Possible ranges per axis |
| Data rate | Record Pi2 waves | 2 (3 component vectors) | Per second |
| Power | N/A | <4 | W |
| Size | Simplicity of installation | $22 \times 13 \times 5$ | cm × cm × cm |
| Sensor design | Survivability in arctic conditions | Ruggedized all weather | |
| Data retrieval and firmware upload | Flexibility of operation | USB interface | |
| | | **Enclosure** | |
| External operating temperature | Operate during winter cold. Survive full sunlit summer days | −50° to +40°C | °C |
| Maintained internal temperature | Commercial electronics operating temperature | 20° ± 10°C | °C |
| Heating power | Minimize utility costs | <150 | W |
| Environmental protection | Survive/operate extreme weather conditions | Hermetically sealed unit w/ nitrogen purge and sealed electrical connectors | |
| Optical $I/F$ with ambient | Good optical transmission | Polycarbonate/acrylic dome | |
| Mounting | Optic axis to be vertical within 1° | Flexible mounting with in field leveling adjustment | |
| Thumbnail data rate (out) | Retrieve thumbnails | 1.23/ continuous (2.7 kbits/s) | Mbytes/h |
| Data rate (in) | Accept $s/w$ uploads | 50 | kbit/s |
| Full image data rate (out) | 20 full images per minute | 2.5 | Mbits/min |
| Storage | On site image archive | 1.2 | Gigabit/day |
| | | **GPS receiver** | |
| Configuration | Timing and geolocation | Integrated antenna and electronics package | |
| Remoteness from host computer | Flexible for installation | >30 | m |
| Time accuracy | Substorm timing <1 s | 1 (NTP compatible) | ms |

**Table 2** GBO stations. Columns 1–6 are self explanatory. Column 7 is the UT time at local magnetic midnight, Column 8 is the serial number of the imager, Col. 9 is the serial number of the GBO electronics, Col. 10 the type of magnetometer and Col. 11 the station installation date

| 1. No. | 2. Site | 3. Abbrev. | 4. Latitude | 5. Longitude | 6. Mag. latitude | 7. Mag. longitude | 8. Mag. midnight (UT) | 9. ASI# | 8. GBO# | 10. GMAG type | 11. Deploy date |
|---|---|---|---|---|---|---|---|---|---|---|---|
| 20 | Goose Bay | GBAY | 53.316 N | 299.540 E | 60.73 N | 23.08 E | 3:37 | 03 | GBO-14 | GMAG-6 (10532/5009) | Feb-06 |
| 18 | Kuujjuaq | KUUJ | 58.155 N | 291.468 E | 66.89 N | 13.23 E | 4:15 | 13 | GBO-13 | GMAG-8 (10547/5011) | Nov-07 |
| 19 | Chibougamau | CHBG | 49.814 N | 285.581 E | 59.57 N | 3.62 | 4:49 | 16 | GBO-17 | GMAG-9 (10546/5013) | Sep-06 |
| 16 | Sanikiluaq | SNKQ | 56.536 N | 280.769 E | 66.45 N | 356.99 E | 5:12 | 09 | GBO-22 | NRCan w/ GPS-9 | Oct-06 |
| 17 | Kapuskasing | KAPU | 49.392 N | 277.680 E | 59.76 N | 351.95 | 5:29 | 21 | GBO-15 | GMAG-7 (10545/5012) | May-06 |
| 10 | Rankin Inlet | RANK | 62.828 N | 267.887 E | 72.41 N | 335.74 | 6:24 | 12 | GBO-09 | CGSM w/ GPS-4 (10528) | Sep-05 |
| 13 | Gillam | GILL | 56.354 N | 265.344 E | 66.18 N | 332.78 E | 6:34 | 19 | GBO-19 | CGSM w/ GPS-7 (10516) | May-06 |
| 15 | Pinawa (LdB) | PINA | 50.163 N | 263.934 E | 60.08 N | 331.46 E | 6:38 | 18 | GBO-16 | CGSM w/ GPS-8 | May-06 |
| 14 | The Pas | TPAS | 53.994 N | 259.059 E | 63.27 N | 323.80 E | 7:05 | 08 | GBO-06 | GMAG-1 (10505/4001) | May-05 |
| 11 | Fort Smith | FSMI | 59.984 N | 248.158 E | 67.38 N | 306.64 E | 8:06 | 10 | GBO-10 | CGSM w/ GPS-3 (10527) | Jul-05 |
| 12 | Athabasca | ATHA | 54.714 N | 246.686 E | 61.98 N | 307.76 E | 8:07 | 02 | GBO-02 | NRCan w/ GPS-0 | Aug-04 |

**Table 2** (*Continued*)

| 1. No. | 2. Site | 3. Abbrev. | 4. Latitude | 5. Longitude | 6. Mag. latitude | 7. Mag. longitude | 8. Mag. midnight (UT) | 9. ASI# | 8. GBO# | 10. GMAG type | 11. Deploy date |
|---|---|---|---|---|---|---|---|---|---|---|---|
| 7 | Ekati | EKAT | 64.717 N | 250.667 E | 72.28 N | 307.66 E | 8:02 | 04 | GBO-04 | GMAG-3 (10503/4003) | Dec-04 |
| 9 | Prince George | PGEO | 53.815 N | 237.172 E | 59.13 N | 295.67 E | 8:52 | 15 | GBO-03 | GMAG-2 (10501/4002) | Sep-04 |
| 8 | Fort Simpson | FSIM | 61.762 N | 238.779 E | 67.30 N | 293.85 E | 8:57 | 05 | GBO-21 | CGSM w/ GPS-6 (10539) | Nov-06 |
| 6 | White Horse | WHIT | 61.010 N | 224.777 E | 63.66 N | 278.14 E | 10:01 | 07 | GBO-07 | GMAG-4 (10533/4015) | Jul-05 |
| 5 | Inuvik | INUV | 68.413 N | 226.230 E | 71.23 N | 275.09 E | 10:17 | 17 | GBO-08 | GMAG-11 (10550/5017) | Jun-05 |
| 1 | Gakona | GAKO | 62.407 N | 214.842 E | 63.06 N | 269.02 E | 10:48 | 20 | GBO-18 | GI w/ GPS-10 | Aug-06 |
| 2 | Fort Yukon | FYKN | 66.560 N | 214.786 E | 67.24 N | 266.14 E | 11:00 | 14 | GBO-12 | GI w/ GPS-5 (10529) | Oct-05 |
| 3 | Mcgrath | MCGR | 62.953 N | 204.404 E | 61.72 N | 259.84 E | 11:32 | 11 | GBO-11 | GMAG-5 (10525/4016) | Aug-05 |
| 4 | Kiana | KIAN | 66.971 N | 199.562 E | 65.13 N | 253.47 E | 12:02 | 22 | GBO-20 | GMAG-10 (10554/4009) | Sep-06 |
| Spare | Berkeley | BERK | 37.881 N | 237.756 E | 43.19 N | 301.21 E | 8:38 | 01 | GBO-05 | GMAG-0 (proto s/n 1) | Mar-05 |

**Table 3** The name, location, abbreviation, IP address, altitude, longitude and latitude of the Education and Public Outreach (EPO) magnetometers. These instruments—besides providing high quality magnetic data—are used by teachers and students in high school science courses

| City | State | Acronym. | Latitude | Longitude | Mag. latitude | Mag. longitude |
|---|---|---|---|---|---|---|
| Bay Mills | MI | BMLS | 46.24 | −84.34 | 56.760 N | 11.15 W |
| Carson City | NV | CCNV | 39.19 | −119.8 | 45.071 N | 57.006 W |
| Derby | VT | DRBY | 44.95 | −72.13 | 55.039 N | 6.015 E |
| Fort Yates | ND | FYTS | 46.09 | −100.68 | 55.756 N | 35.281 W |
| Hot Springs | MT | HOTS | 47.61 | −114.67 | 54.730 N | 53.498 W |
| Loysburg | PA | LOYS | 40.18 | −78.38 | 51.063 N | 3.367 W |
| Pine Ridge | SD | PINE | 43.08 | −102.59 | 52.439 N | 37.396 W |
| Petersburg | AK | PTRS | 56.83 | −133.16 | 59.910 N | 76.67 W |
| Remus | MI | RMUS | 43.66 | −85.14 | 54.647 N | 12.992 W |
| Shawano | WI | SWNO | 44.78 | −88.60 | 55.31 N | 17.400 W |
| Ukiah | OR | UKIA | 45.14 | −118.93 | 51.317 N | 57.711 W |
| San Gabriel | CA | SGD1 | 34.20 | −117.85 | 40.376 N | 53.632 W |
| Table Mountain | CA | TBLE | 34.38 | −117.68 | 40.596 N | 53.493 W |
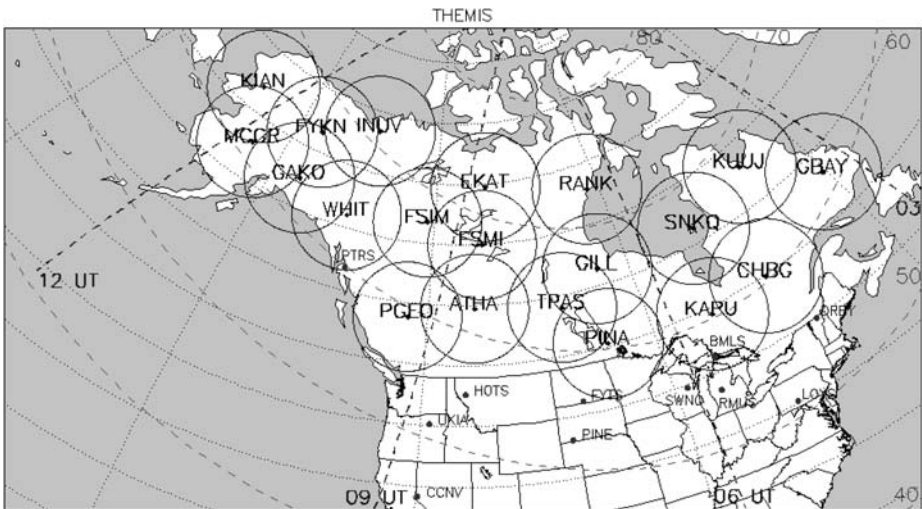


**Fig. 5** Map of North America with the GBO station names, locations and their approximate fields of view of the all-sky cameras. Magnetic latitudes are shown with *dashed lines*. Meridians of local magnetic midnight at 03, 06, 09, and 12 UT are also indicated

image, the intensity of only one of the pixels is used. This procedure does not make use of the ultimate SNR obtainable from the co-adding of multiple pixels, however, in general there is no point in enhancing the SNR in small selected region of the image. In cases when several latitude/longitude bins correspond to a single all sky pixel the same intensity is used repeatedly for all the bins.

**Fig. 6** Schematic showing the cross-sectional view of the all-sky imager, illustrating that equal distance on the "sky" at auroral altitude, $dx$, represents progressively smaller angles, $d\theta$, towards the horizon
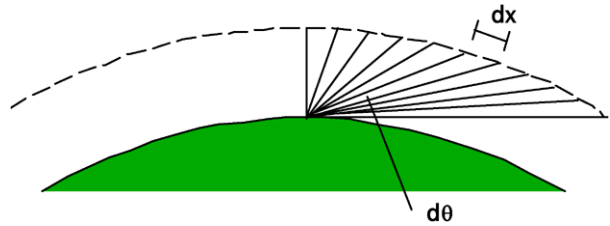


**Fig. 7a** All-sky image of arcs near the poleward edge of the aurora oval taken at a time when the FAST satellite passed through. The image was taken at Rankin Inlet Station. The *small white crosses* represent the FAST positions at each full minute starting at the top at 03:20 UT
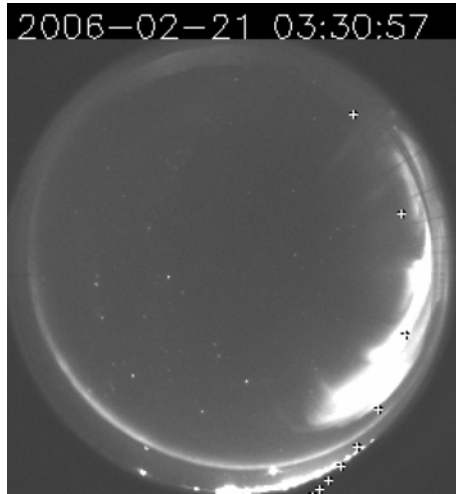


**Fig. 7b** The same all-sky image backward-projected and shown on a geographic latitude longitude grid
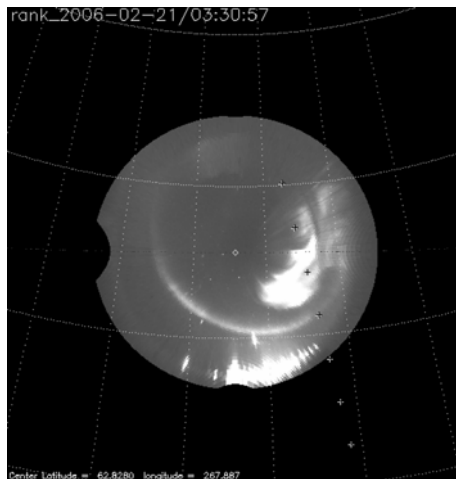


Mathematically if the latitude/longitude bins are represented by coordinate system $x_0$ and $y_0$ and the all sky image pixels by $x_i$ and $y_i$ then the intensity in the output bin:

$$I(x_0, y_0) = I(x_i, y_i) = I(f(x_0, y_0), g(x_0, y_0))$$

**Fig. 8a** A forward projected all-sky image demonstrating that, although near its center there is complete coverage, towards the edges only some pixels are illuminated. This is because each pixel in the output image represents larger and larger areas of the "sky"
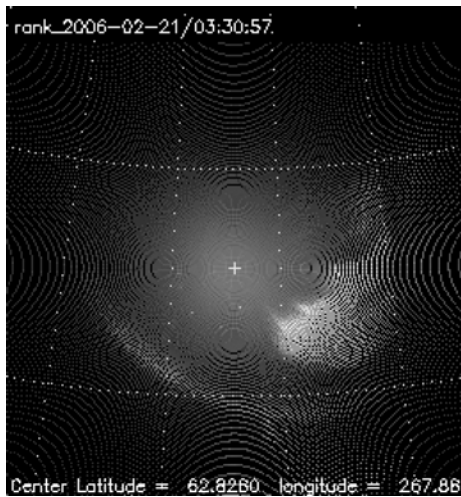


**Fig. 8b** If the image were divided into 1024 approximately equal area bins, on the sky the *white dots* would signify the corners of the projection of the bins on the original image
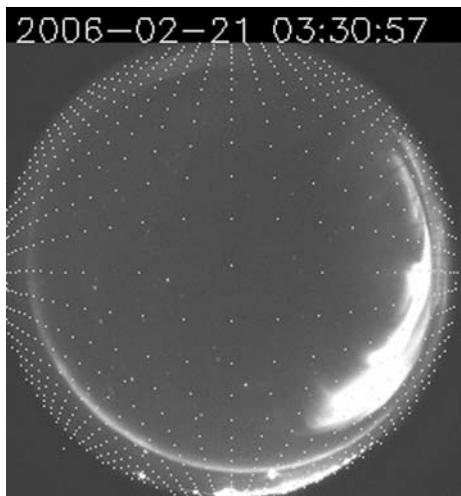


where the functions $x_i = f(x_0, y_0)$ and $y_i = g(x_0, y_0)$ define the image pixel coordinates in terms of the corresponding output bin coordinates.

Figure 8a presents the same image in a forward-projected transformation, in which pixels in the original image (see Fig. 7a) are transformed to the 110 km altitude region and then projected onto a latitude/longitude coordinate system. On a $256 \times 256$ output image matrix, not all pixels receive information due to the coarseness of the grid. Upon close inspection, this image is sparsely populated with light, especially near the outer regions.

Figure 8b illustrates how a matrix of similar size bins of approximately 30 km $\times$ 30 km projected on the sky would translate to various size bins on the original image. Each white point on the image represents the corners of approximately equal area bins at 110 km altitude on the "sky."

The minimization of the data volume for NRT transmission to the home base was a high priority. We use a data compression scheme that takes advantage of the fact that the all-sky cameras over sample the central region of the image. In this scheme, a 1024-element

vector is generated from the all-sky images, where each element represents the intensity of an approximately equal area regions of the aurora. These vectors are transmitted through the internet.

Upon receiving the data. the 1024-element vectors are converted into reduced resolution thumbnails. These thumbnails satisfy the Level 1 requirements of the THEMIS GBO program because they retain the spatial and temporal resolution necessary to locate and time the substorm onsets. The thumbnail images permit the construction of quasi global auroral images, so-called mosaics. These mosaics are produced as soon as the NRT data are received through the internet—usually with less than one day delay.

## 4 GBO Instrumentation: The All-Sky Imager (ASI)

There were two primary considerations in the imager design. The first was to satisfy the THEMIS scientific requirements. The second was to keep the cost of each camera well under $10,000 so the program could afford the large number (20) of them. This reduction in cost was made possible by using a white light (panchromatic imager). Because the THEMIS science does not require accurate quantitative measurements of the auroral light in the various different wavelength bands, it was possible to use a white light imager.

In the past decades, filtered all-sky imagers based on the telecentric scheme of Mende et al. (1977) became accepted as the standard. With the use of a filter, an auroral spectral feature can be isolated. The measured photon flux can be meaningfully interpreted in terms of the auroral brightness in absolute units such as Rayleighs (Chamberlain 1961). Unfortunately, when filtering is applied, the resultant light from the aurora usually becomes so faint that the systems operate in a photon-starved mode and un-intensified CCDs are generally unsuitable detectors. To illustrate this, consider a CCD with a measured readout noise of 10 electrons r.m.s. (root mean square), which means that it will need 30 signal electrons to have a signal-to-noise ratio (SNR) of 3. In the detection of auroras, filtered auroral images may contain no more than 2 to 3 photo electrons per pixel, which would be undetectable by an unintensified CCD. However, the same signal would be quite visible with an intensified system which has intensification gain in front of the CCD. Thus the introduction of a narrow band filter in auroral observations almost always requires the use of some kind of intensification in front of the CCD. Unfiltered auroral imagers, like the THEMIS ASIs, collect light in the entire visible range and the signal is almost 10 times the intensity of any single auroral spectral feature. Thus the 2 to 3 photo electrons of a single spectral feature would be equivalent to 20 to 30 electrons in white light—just about detectable by an un-intensified CCD that has 10 electron r.m.s. noise. To minimize system complexity in the THEMIS camera design, we were able to stay away from intensification without compromising the instrument performance.

By using the white light system, do we abandon all possibility of quantitative interpretation? To answer this question we have modeled the spectral profile of auroral emissions due to different energy electrons (Lummerzheim and Lilenstein 1994; Chaston et al. 2005) and simulated the collection efficiency of a typical white light video camera of the type described by Maggs and Davis (1986). We found it quite remarkable that in most cases the camera signal was closely proportional to the observed auroral precipitated energy.

Figure 9 shows the results of the modeling for this type of camera. In general, the response is close to unity for all energies higher than 3 keV, indicating that in this energy range a white light camera provides data that is a good measure of the total precipitated energy. The legend shows the different assumptions that were made for magnetic activity,

**Fig. 9** This shows the modeled camera white light response in equivalent kR, based on the properties of a camera described by Maggs and Davis (1986) for different atmospheric conditions. By modeling three different types of auroral electron precipitation spectra—a 0.5 Maxwellian, a 5 keV monoenergetic and a 10 keV monoenergetic—three points were generated and the points were connected by lines



**Imager Responsivity**
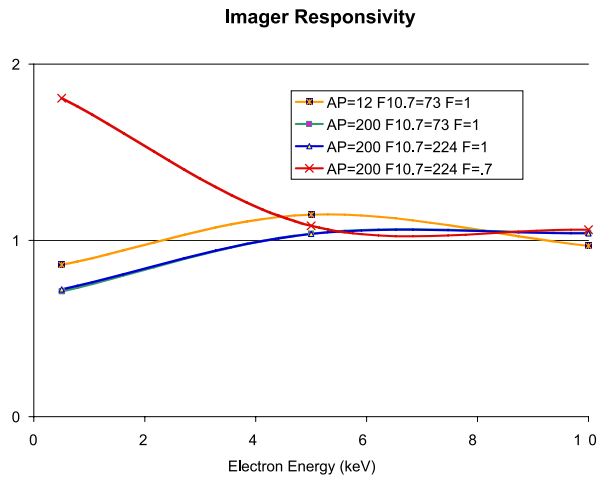
such as $A_p$ and $F/10.7$ indices used in the modeling. The $F$ factor in the atmospheric model (MSIS-90) is used to investigate the dependence on the atmospheric O/N$_2$ ratios when they are different from the nominal atmospheric model. The O scale-height in the model was reduced to 70%. This was an unrealistically drastic reduction showing that the response was significantly enhanced at low energies. Presumably this is because low energy electrons are more efficient in producing white light when interacting with N$_2$ rather than O atoms. In most studies the dependence of auroral emission efficiency on the atmospheric composition is rarely accounted for (Hecht et al. 2006).

Using white light imaging gave us the following major advantages, simplifications and corresponding cost savings:

(1) No expensive filters were needed.
(2) No mechanisms were required for changing filters (e.g., filter wheels) or complex wedge prisms in order to split the light between various wavelengths.
(3) The large bandwidth provided large gains in photon collection and allowed the use of short (1 s) exposure times with very high SNR, even with faint aurora.
(4) Since the system was not "photon-starved," there was no requirement for image intensification with such complexities as a high voltage system and daylight protection.
(5) The white light images had good SNR for many stars, permitting the geometric and intensity calibration and monitoring of the weather conditions above the imagers.

In summary, a simple wide field-of-view optical system, black and white CCD camera operating with a 1-second duration exposure satisfied all the requirements. We built a prototype all-sky imager and tested it. In our first prototype, there were no moving parts, just the passive optics, the camera and a computer.

The basic design of the THEMIS all-sky camera (Mende et al. 1977) was originally developed to record narrow-band evenly-filtered images of the whole wide all-sky camera field. Although filtering was not a requirement for THEMIS, other considerations still favored this same design. For example, it allows use of the inexpensive mass-produced fisheye lenses commonly used with 35 mm format cameras. These lenses were available with moderate speeds ($F/3.5$) and could be obtained readily. The design permits attachment of such lenses to a wide range of different size CCD cameras with inexpensive coupling optics. The Peleng $F/3.5$ 8 mm focal length lens was selected. Its large format image was

**Fig. 10a** A schematic
cross-section of the all-sky
imager (ASI)



1.Dome
2.Fish eye lens F/3.5
3.Telecentric Lens
4.Bandpass filter (Optional)
  (In THEMIS IR suppression)
5.Intermediate image
6.Field lens
7.Re-imaging objective F/0.95
8.CCD camera
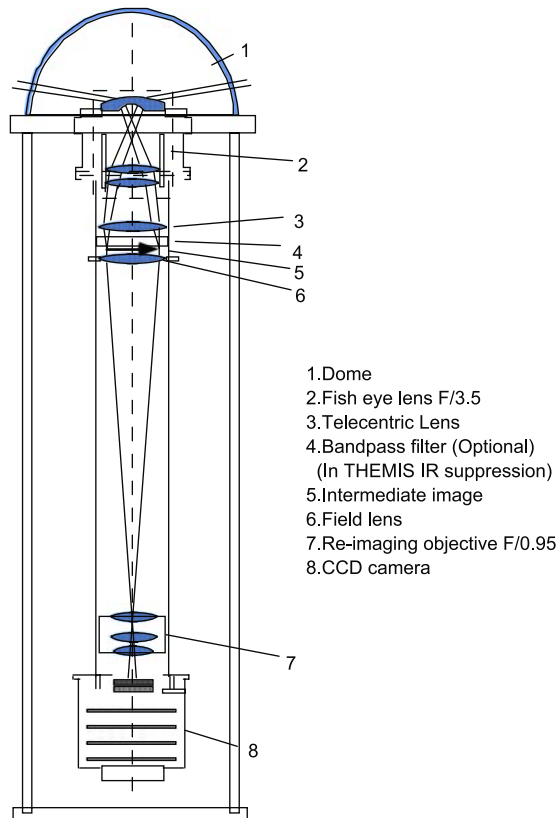
de-magnified and projected on the CCD by the combination of a closeup lens and a Canon $F/0.95$ 25 mm Soligor lens. This arrangement resulted in an all-sky system that uses only inexpensive mass-produced lenses, while having an overall system speed of $F/0.95$, coupled with excellent resolution. Our estimates show that the camera should produce about 100 electrons per pixel per kilo Rayleigh during the selected 1-second exposure. Twenty-two of these relatively inexpensive camera systems were built. They had sufficient sensitivity to detect less than 1 kR aurora with an exposure duration of 1 second. These cameras were about fifty times more sensitive than the IGY cameras, which required long (55 s) exposures. The sensitivity and resolution of the system is adequate to record fairly deep starfields for calibration.

In the THEMIS cameras, the telecentric filter space was used to include a heat-reducing infrared (IR) suppression filter. The camera is illustrated in Fig. 10a. The camera is under the dome (1) in a hermetically sealed aluminum chamber with internal thermal insulation. The Peleng fish eye lens (2) is followed by a simple condenser lens, which also serves as a telecentric lens (3) ensuring that the rays coming from the Peleng lens exit pupil are approximately parallel with the optic axis while passing through the filter. This lens moves the apparent center of the Peleng lens exit pupil far away to "infinity," hence the name "telecentric." An intermediate image (5) is formed near the filter. Another simple field lens (6) directs all the rays into the entrance pupil of the $F/0.95$ re-imaging lens (7). There is a 2-diopter closeup lens (not shown) in front of the re-imaging lens (7) so that the lens operates nearer to infinity conjugate to where its operation was optimized. The CCD camera is a Starlight

**Fig. 10b** Photograph of the actual camera unit assembled

**Fig. 10c** As installed on the roof
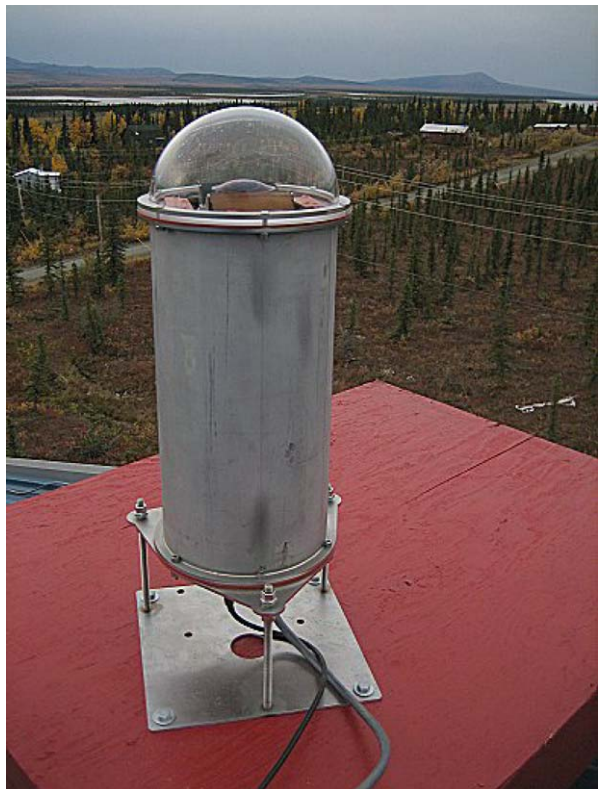
Express camera containing a Sony black and white CCD, with a USB output connection to the computer.

Heaters, temperature sensors and other auxiliary items are packaged in the camera housing. The sun exclusion shutter is the only moving part of the system. The first prototype imager was installed and operated without a shutter in Athabasca for a whole year as a trial operation. Some of the coatings and the interior paint of the lens deteriorated noticeably during this first year. It was thought that the lifetime of the cameras could be greatly extended if they were protected from continuous year-round direct daytime sun exposure. Furthermore, the CCD has a plastic microlens array in front of the sensitive area and the plastic may be subject to UV degradation. Although none of these deleterious affects made any noticeable change in the camera operation for the first trial year, a mechanical clamshell shutter was designed and installed on each camera as a precautionary measure. The ASI array should be in operation for several years and these shutters should prevent the cumulative effects that might be more significant over several years. The design was "fail-safe" because the shutter has to be powered to close, and it is most likely to fail in the open position.

## 5 The THEMIS GBO Magnetometers

The GBO fluxgate magnetometer system consists of the sensor—normally buried in the ground—and the auxiliary electronics box located in the electronics enclosure. The sensor is connected to the support electronics via an extended cable threaded inside a garden hose, which provides effective protection of the cable at a modest expense. The sensor is protected by waterproof housing made of plastic pipe.

The magnetometer (GMAG) electronics contain the GPS receiver, which is used to generate time stamps for the GBO data products. The magnetometer auxiliary electronics are illustrated schematically in Fig. 11. The sensor cable connector (on the right) provides the drive signal from the generator to the fluxgates. The 3 sense axes are first amplified and then
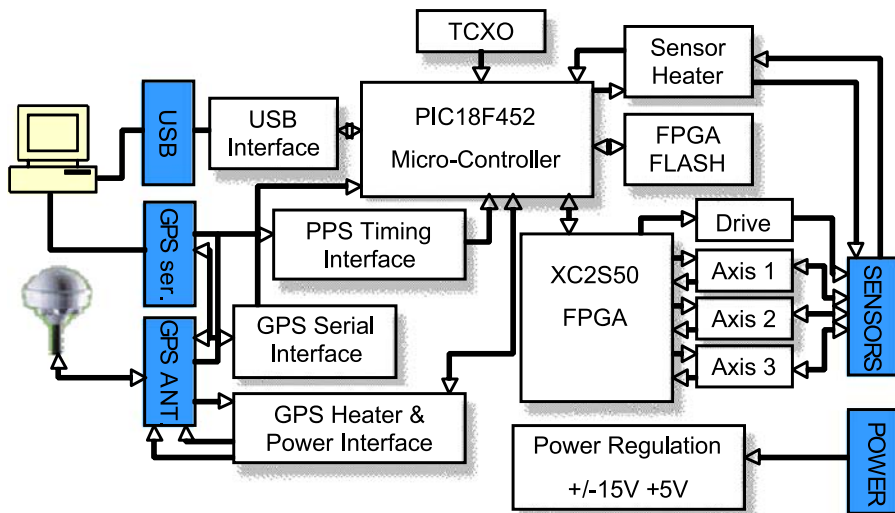


**Fig. 11** GBO magnetometer system diagram

digitized in the Field Programmable Gate Array (FPGA). The data are transmitted to the GBO station processor by the micro controller, through a USB interface. The GPS signals are processed and sent to the GBO computer via a serial line. The whole system was built and calibrated by UCLA.

## 6 The THEMIS GBO Station Design

Figure 12 illustrates the station design. The science detectors are the All-Sky Imager (ASI) and the magnetometer (GMAG). They produce the science data stream, which is transmitted to the GBO processor. The GPS receiver generates more accurate timing than the THEMIS requirements demand (∼1 s). The internet serves as the data retrieval and command channel at any station where wired high speed internet is available. At other stations, where high speed internet is still not available, a synchronous satellite-based internet service system was installed. This required a local transmitting and receiving station with an associated dish antenna (Telesat dish illustrated in Fig. 12). At some sites, an additional Iridium satellite transmitter/receiver was also installed to send commands or receive low-rate and housekeeping data.

A typical installation is shown in Fig. 13. The photograph was taken in Athabasca (ATHA). The station at Athabasca has several optical instruments, and the bigger dome on the roof is not related to THEMIS—the THEMIS GBO ASI is the small white unit to the right of the big dome and has a small dome on it. In front of the building, the white box is the computer and auxiliary electronics environmental housing. Most of the magnetometer sensor head is buried except its top, which is clearly visible in the foreground.

At each site, the installation configurations can be different. The computer hardware is situated where a conveniently-located building exists. The camera is in its own cylindrical environmental housing, either on the roof of the building or somewhere nearby mounted on a pole or a tower. The camera housing is hermetically sealed to keep out dust and humidity.
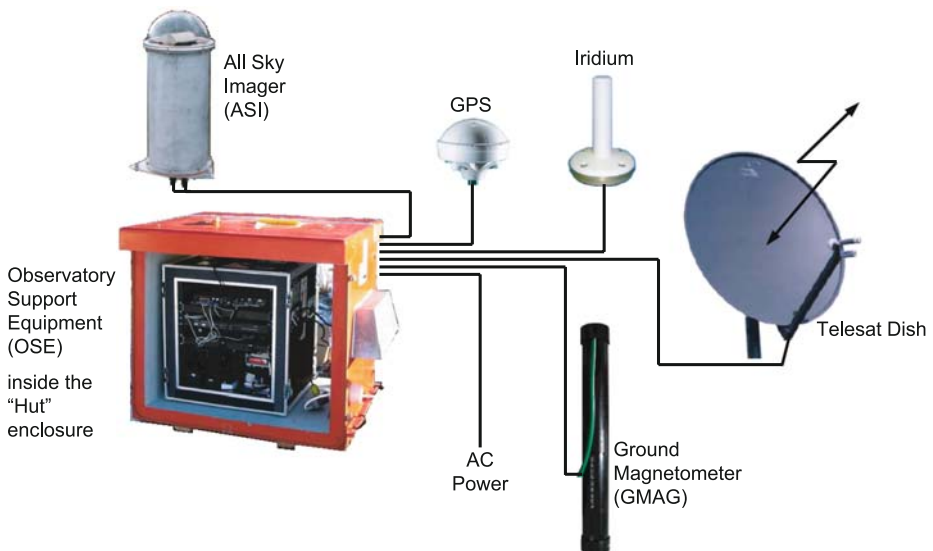


**Fig. 12** GBO station schematic

**Fig. 13** GBO station as installed in Athabasca, Canada



It is made of aluminum with a layer of insulation inside and the dome is made of clear acrylic.

The availability of a suitable shelter determined the enclosure selection for the computer and auxiliary electronics at each site. If a building was available, then the GBO electronics were installed in their portable 19-inch rack (Fig. 15) without any additional protection. In this configuration, the ambient room temperature took care of the thermal requirements. In cases where no shelter was readily available, a special environmental fiberglass enclosure was installed to protect the GBO auxiliary electronics. It was relatively simple to add heat and keep a reasonable temperature inside the environmental enclosure during cold weather, using power available at each site from the local power grid. A much greater challenge was thermal conditioning the enclosure during the summer hot weather. The heat generated by the electronics, including the computer, needed to be conducted outside of the enclosure through the insulating shelter walls. A solid state thermal electric cooler was installed in one of the walls of the environmental enclosure to satisfy this requirement. This cooler had sufficient power to handle the heat generated by electronics inside the shelter.

The electronics enclosure had an active temperature control system to regulate the heaters and the thermal electric cooler. In Fig. 14, we show a schematic of the auxiliary electronics of the GBOs. The ASI and the GMAG are connected to the system computer via USB interface. The GPS data are provided through a serial input into the computer. The heart of
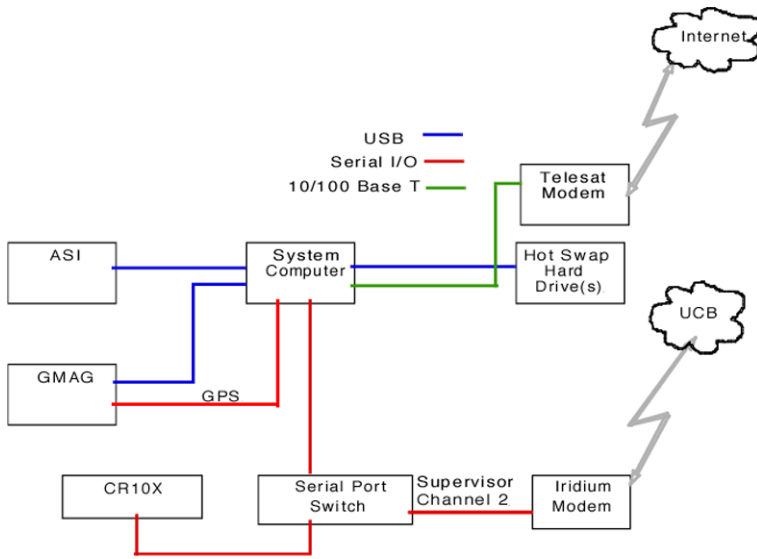
**Fig. 14** Schematic of GBO support electronics
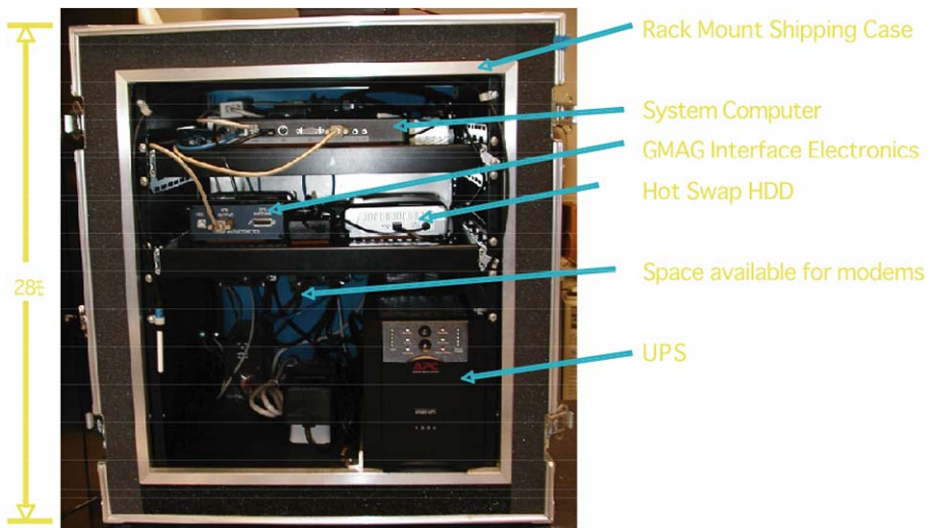


**Fig. 15** Photograph of GBO support electronics

the environmental control system is the CR10X micro-controller. This is a programmable controller, it has temperature sensor inputs and can turn on and off heaters and other equipment. This device has been qualified over a wide operating-temperature range and uses minimal power. It has its own battery backup system, which provides uninterruptible operation for several weeks. A major advantage of the system is that it can be re-programmed remotely through one of the communication systems—either the internet or the Iridium system (Fig. 14). For example, the temperature setpoints, where heaters and coolers turn on

or off, can be changed without visiting the site. In addition, the CR10X permits turning off the system computer if the system overheats. The system computer uses substantial power because it has to process and compress the image data into thumbnails in real time for transmission via the internet. One of the peripherals of the system computer is the Hot Swap hard drive. When this drive is full, the custodian physically disconnects it and sends it back to the University of Calgary. The rack mount enclosure (Fig. 15) is part of every GBO electronics subsystem.

## 7 The THEMIS GBO Data

The time resolution requirements dictate the retrieval of large data sets. The GBO ASI data system supports a fast, three-second cadence with each image having $256 \times 256$ pixels. Twelve to fourteen bits intensity resolution is required to cover the large dynamic range of the aurora. The full image data collected every three seconds result in a ∼2.5 MB/min continuous data stream per station. For 20 stations, this represents ∼50 MB/min of combined data rate. It would not be possible to reliably retrieve these data from our remote sites via the internet. Therefore, we adopted two separate data retrieval methods. All images were stored at the site, for later retrieval by physically mailing back the hard drives. For NRT data transmission through the internet, a compressed version was generated, consisting of 1024 vector elements per image. The vector data stream is produced from the CCD images via address lookup tables at each site. This data stream provides adequate spatial resolution to satisfy the THEMIS Level 1 requirement and publish the data in near real time.

The THEMIS data retrieval system is schematically illustrated in Fig. 16. Some of the data are retrieved via the internet, as shown by solid black arrows. The full resolution images cannot be retrieved this way and they are recorded on-site on external USB hard drives. The various data products are shown schematically at the bottom of Fig. 16. The global mosaics are produced at Calgary from the thumbnails and later on from the full images. Several "browse products" will be produced from both types of retrieved data and will be available online through a standard internet browser. The team is also committed to producing CDF



**Fig. 16** THEMIS data flow and summary of GBO data types

data files from both the thumbnails and the full images. The mission summary plots contain GBO-derived keogram data in addition to the key satellite data displays. The magnetometer data are available both as data plots and as sets of downloadable CDF files.

We distinguish the two types of data: (1) the near real time thumbnail image data, real time keograms produced at the sites and hourly images and magnetometer data to be retrieved electronically via internet on a daily basis and (2) full resolution image data that will be copied from hot swap hard drives mailed back from the sites.

The NRT data will be transmitted daily to UCB by internet via a main node at the University of Calgary. Those data consist of thumbnails images reconstructed from the 1024 vectors, keograms and hourly full resolution images. The latter two are jpeg images, which are also useful as engineering data with which to monitor station health. These are not converted to CDF format. They are available for viewing on the web in their native jpeg format. The daily and hourly keograms (32 or 256 pixel vertical scans at 1-min or 6-s cadence) and the thumbnails (at 3-s or 6-s cadence) are the highest temporal resolution data possible given the available bandwidth used in the retrieval.

The high-resolution data stored at the site is retrieved by the local custodians periodically (1–3 months). The drives from the stations are sent to the University of Calgary and subsequently to UCB by mail, where they are copied and archived on servers for retrieval. The ASI hard drive data consist of high spatial resolution $256 \times 256$ pixels images at the highest time resolution (3 s).

Both data types are processed to serve as THEMIS GBO data products accessible on the web.

## 8 Description of the THEMIS-GBO Web-based "Browse Products"

The thumbnail ASI and GMAG data from all stations are collected by the University of Calgary through the internet. The magnetometer data will be passed to UCLA for validation. The magnetometer data are included in the THEMIS GBO data products. The first six browse data products are created from the NRT data.

*Data Product 1*    Hourly full average and jpeg compressed 1-minute images. Once an hour, a full jpeg image is transmitted from each GBO site. This format is intended for data quality evaluation, including assessment of the sky clarity over the station. Once a minute, a jpeg compressed full image is also retrieved.

*Data Product 2*    Clickable KEOGRAMS. A set of Keograms are produced at each GBO station from the full resolution images. These are transmitted as separate files. An example of the available Keograms from all stations is shown in Fig. 17 in collage form. On the THEMIS science operation center (SOC) web display, these Keograms are accessible directly. Clicking at any UT time, displayed as the horizontal axis on the Keogram, will open one of the GBO summary images (Data Product 3) for the appropriate time and station from the THEMIS gifs produced from the images.

*Data Product 3*    GBO summary images. This is a set of gif images produced first from the thumbnails that contain 1024 pixel vectors. As the full data sets become available from the mailed hard drives, the thumbnail gif images are replaced with gifs produced from the full fidelity images. On the Keogram in Data Product 2, in the very rightmost column, the presence of the "*T*" indicates that the gif images still represent the thumbnail data. A click on the Keogram will reveal the appropriate hour data as a collage of gif images taken on the even minute. Clicking on any one image will expand it to the full time resolution (3-s cadence) or 20 gif images per minute.
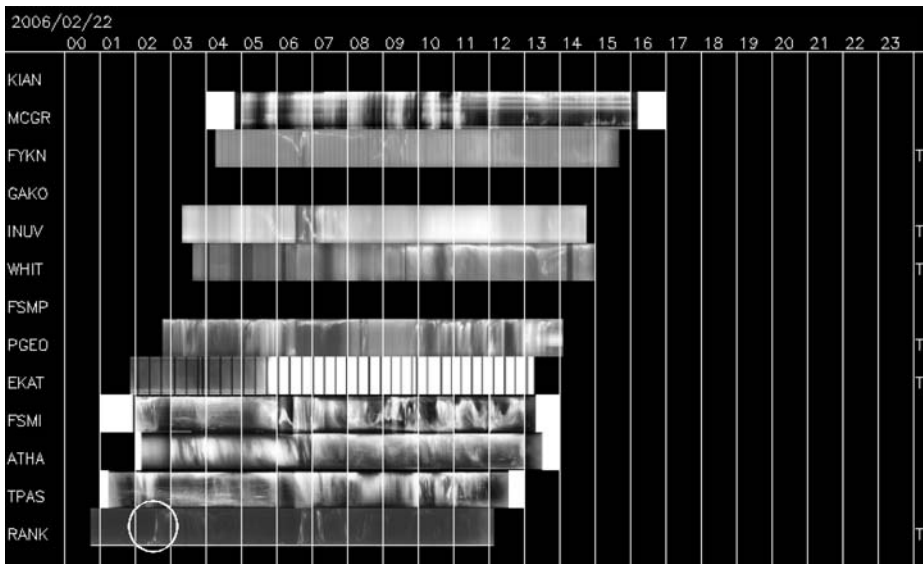
**Fig. 17** Keograms from the available stations for February 21, 2006. Clicking on the Keogram derived from Rankin Inlet Data (RANK) hour 2–3 UT (marked with *black circle*) will produce the full resolution collage of Fig. 18a

*Data Product 4* Magnetometer data. Individual magnetometer station data *X*, *Y*, and *Z* components are presented as a function of time.

*Data Product 5* Mosaic. Full mosaics are produced for the entire array from the thumbnail images or, when available, from full images. These data products are available about 2–4 days after data collection.

### 8.1 THEMIS Downloadable CDF Files

In addition to the "browse products" described here, the THEMIS science operation center will produce downloadable CDF files. If the science requirement is simply to view images, then the browse products will suffice in most cases. However, if further processing of the GMAG or the ASI data are required, then the CDF files described below will be most useful.

The THEMIS data Level 1 (L1) will be in CDF file format. The THEMIS team provides the community with additional calibration files. The team also provides software tools that read these files and plot the data in a scientifically useful way, producing plots of physical quantities. The software can support integrated analysis and combined plotting with the rest of THEMIS data products. Derivative of the L1 data files, the L2 files are created. These are used in NSSDC data center, facilitating further distribution and plotting through CDAWeb capabilities.

All CDF files are processed at UC Berkeley and University of Calgary independently, but using common processing code, in order to adhere to the same format and file structure described herein. The same structure is intended for use by future ancillary data sets, as they become available. All ASI data will be transformed into 16 bits before they are written to L1 data files. The three types of CDF L1 data products are shown in Table 4.

The first L1 data product is the high time resolution Keogram produced from the 3-s cadence full spatial resolution data. The second data product is comprised of the thumbnail

**Fig. 18a** One hourly image collage from the full resolution images. Clicking on minute 50 (shown with *circular frame*) will open the full time resolution collage, which is illustrated as Fig. 18b
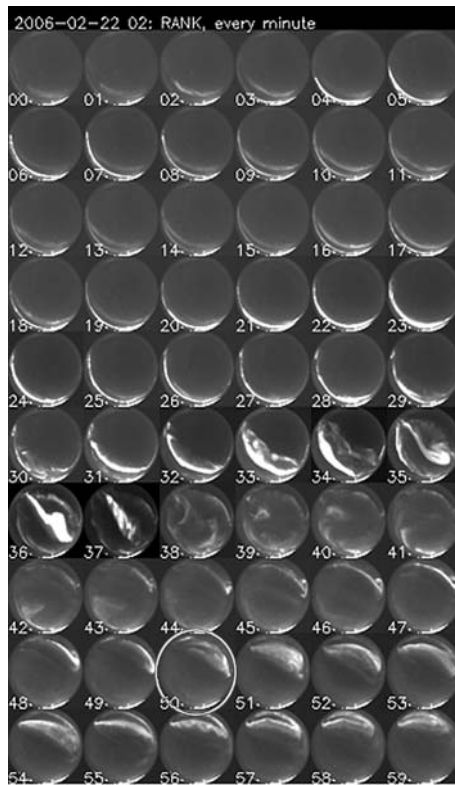


**Fig. 18b** Full time resolution 3-s cadence, 20 images per minute
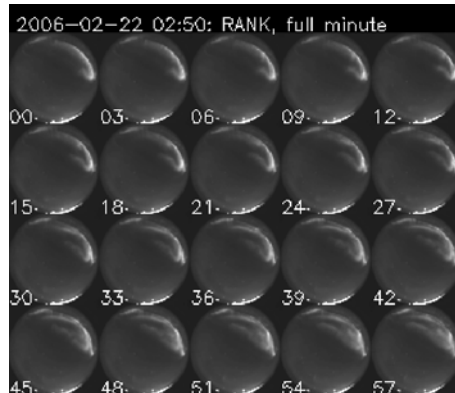


images at full time resolution. Some of the stations have reduced transmission bandwidth and the near real time data will only support 6-second cadence or 10 exposures per minute. When the full resolution data are retrieved via the mailed hard drives, then the missing alternate frames can be filled in and full time resolution can be restored with 20 frames per minute. The last L1 CDF set is the full images after they have been copied off the returned hard drives.

**Table 4** ASI Level 1 data types and their file names

| | L1 VARNAME | Width (pixel) | Frame height (pixel) | Size (bytes) | Cadence (frames/ minute) | Sites (per file) | Hour (Mega bytes) | Day Ave (Mega bytes) | Max (Mega bytes) | Year 20 sites (GB) |
|---|---|---|---|---|---|---|---|---|---|---|
| High T-Res Keograms | thg_ask | 1 | 256 | 512 | 20 | 20 | 12.3 | 98.3 | 295 | 700 |
| High T-Res Thumbnails | thg_ast_ssss | 32 | 32 | 2048 | 10 | 1 | 1.23 | 9.8 | 29.5 | 1391 |
| High T-Res Full frames | thg_asf_ssss | 256 | 256 | 131072 | 20 | 1 | 150 | 1200 | 3600 | 8554 |

| | L1 VARNAME | L1 FILENAME |
|---|---|---|
| High Time Res Keograms | thg_ask | thg_l1_ask_yyyymmdd_vnn.cdf |
| High Time Res Thumbnails | thg_ast_ssss | thg_l1_ast_ssss_yyyymmdd_vnn.cdf |
| High Time Res Full frames | thg_asf_ssss | thg_l1_asf_ssss_yyyymmdd_hh_vnn.cdf |

## 8.2 Example of THEMIS-GBO Observation Data Set Taken on the 23rd of December 2006

The THEMIS GBOs provide a new view of the auroral regions, and allow the unambiguous recognition of the temporal onset from ground-based data. Mende et al. (2007) describes a substorm that occurred on the 23rd of December 2006 that was captured using the THEMIS GBOs and discusses the accuracy of determining the onset location and timing. Mosaics were made from the station images where the sky was clear. To produce the mosaics, the aurora at each station was projected on the "sky" at 110 km altitude. The resulting image collage consisted of a $1024 \times 512$ pixel matrix. Where pixels from image regions of adjacent stations overlapped, the mean of the intensities was taken. This mapping process was only performed once, and a lookup table was generated, allowing subsequent rapid mapping of the entire station array for a selected time period.

For comparison with the optical aurora, the horizontal magnetic vector data were superimposed on the images (Fig. 19). These are the magnetic deviation components produced by subtracting data from a quiet day (December 28, 2006) from each measurement. The arrows represent the horizontal components ($B_x$ in meridional and $B_y$ in east-west [zonal] direction) by the red vectors (Fig. 19). A substorm mosaic movie was made from 06:17:00 to 06:30:00 UT for December 23, 2006, using optical data from six stations (SNKQ, GILL, FSMI, WHI, INUV and FYKN). This can be viewed at: http://www.agu.org/journals/gl/gl0717/2007GL030850/supplement.shtml or ftp://sprite.ssl. berkeley.edu/pub/mende/GBO_movies/12_23_06_movie_quicktime.mov

Prior to onset, the aurora was relatively stationary, with an extended east-west arc located relatively near the zenith at stations SNKQ, GILL, and FSMI. The sky clarity at WHIT was not good enough to assess the situation between FSMI and the Alaskan sector. The latter is clearly seen from the INUV and FYKN data. The arcs were also visible in the Alaskan sector. Another poleward arc system was most visible at FSMI. The magnetic field variations were minimal at most stations, except those that were near the field-of-view of

**Fig. 19** Mosaic presentation of six auroral images from the THEMIS GBO chain. The stations are: SNKQ, GILL, FSMI, WHIT, INUV and FYKN. The magnetic field vectors were superimposed in the manner described in the text. Image times are indicated on the *top left*. 6:17:00—stationery arc structure with low level of magnetic variation. The westward current is somewhat larger at the sector where the breakup will occur. Some enhancement of the westward current is seen (6:18:33), followed by bifurcation of the arc (6:18:48) and the first frame showing the structured arc prior to breakup (6:19:36). The poleward arc feature is still present westward of the surge (6:22:18) and it disappears by 6:21:42. Breakup is in progress and field vectors are east-west and west-east because of strong FAC east and west of breakup. At (6:26:57) apparent substorm onset intensification is seen in Alaska
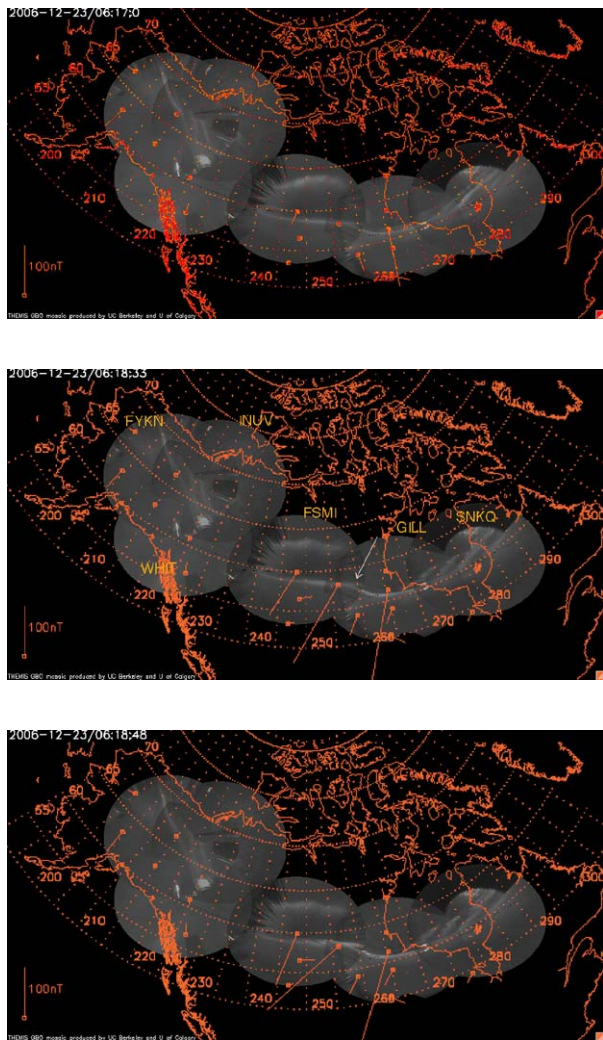


GILL and FSMI where the breakup subsequently occurred (6:17:00). The magnitude was slowly increasing prior to and reaching ∼200 nT at breakup. The deviation was mainly southward, signifying a westward ionospheric Hall current. There was no eastward current anywhere in the region, therefore the location of the Harang discontinuity could not be established.

The first sign of substorm onset was that the equatorward arc began brightening at 6:18:21 UT with simultaneous increase in the westward current. The first morphological change occurred at 6:18:33 UT (Fig. 19), when the arc appeared bifurcated at the eastern sector of the FSMI frame—here indicated by an arrow. Otherwise the morphology did not change significantly until the arc breakup at 6:18:48 UT, unlike the onset observation of Donovan et al. (2006) who found that the auroral brightening was preceded by east-west structuring. Note that Donovan et al. had only single-station ASI observations. They were unable to rule out a non-local onset and the subsequent propagation of the disturbance from

**Fig. 19** (*Continued*)
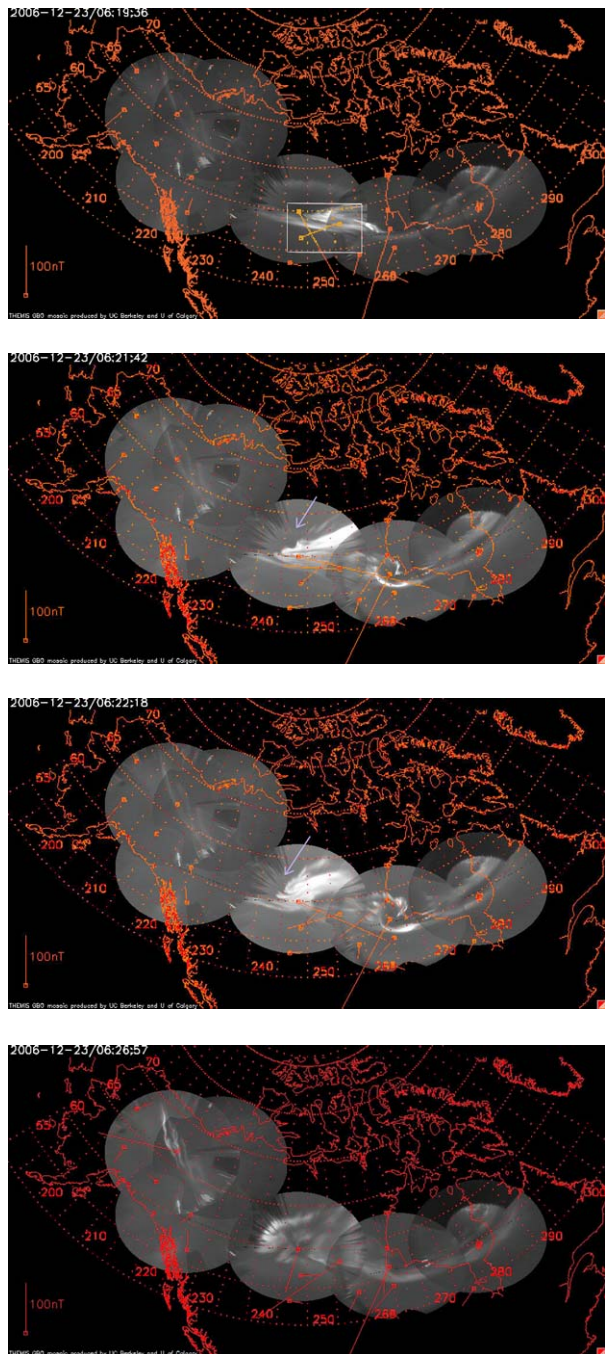


outside of their field-of-view. In our case, the breakup occurred at latitude 58°N and longitude 256°E (67°N magnetic and 22.1 hours MLT) near the region of the bifurcation, and 27 s later than the first discernable brightening. Because the aurora is an east-west elongated

arc, the onset determination is accurate to the nearest degree in latitude, but the longitude could be in error of 2 to 3 degrees.

The 6:19:36 UT image (Fig. 1) shows a significant poleward auroral surge. Superimposed on the image is a rectangle showing oppositely-directed magnetic field vectors at two adjacent stations. Counterflowing (north-south) ionospheric currents could cause such a configuration. However, in this case the scenario is consistent with the superposition of the magnetic field from a vertical field aligned current (FAC) due to the substorm current wedge (Akasofu 1972; McPherron et al. 1973). In fact, the overall distribution of the magnetic variations (06:19:36 UT Fig. 1) is consistent with a model of a current system made up of a westward flowing electrojet current, a vertical upward flowing 500 A FAC centered to the west (61°N, 250°W), and a similar magnitude downgoing FAC to the east (60°N, 268°W) of the onset point.

As discussed earlier, at onset there was a clearly visible arc poleward of the breakup arc. The most poleward arc is often associated with the closed field line region poleward (tailward) boundary, therefore it maps to the nightside steady state reconnection line (e.g. Mende et al. 2003). In our case, this arc is present east and westward of the surge and it becomes fainter on the west side, becoming barely visible by 6:21:42 (indicated with an arrow) at FSMI west of the surge. By 6:22:18 (36 seconds later), this feature disappears, and after that the surge arc is the most poleward feature. It has been found in prior observations involving satellite in-situ and imaging data that, prior to substorm onset, the bright onset aurora is not the most poleward feature. However, later, when the substorm is in progress, the surge arc becomes the most poleward feature. The significance of this is that the most poleward arc is often associated with the last closed field line, therefore it maps to the nightside re-connection line. The disappearance of the poleward arc can be interpreted as the opening of the previously closed magnetic flux. And we interpret the surge arc as the new poleward (tailward) boundary of the closed magnetic flux. This would be topologically consistent with a plasmoid formation and its disappearance downtail (Hones 1972). The subsequent poleward expansion of the surge would be also consistent with dipolarization.

The image at 6:26:57 UT shows a situation where the aurora displays the pre-onset arc in Alaska just prior to its undergoing breakup five minutes later. Subsequent to this image, the aurora underwent a similar breakup in Alaska, with electrojet current intensification and a westward turning of field signature. This illustrates that the large local-time coverage of the multiple GBO stations was necessary in order to correctly identify that the prior onset location was in Canada. In general, the widespread westward turnings of the horizontal magnetic field vectors after onset can be associated with an upward FAC poleward of the stations. This shows that the propagating breakup produced a similar upward-flowing current in the Alaska sector, but some minutes later.

## 9 Summary

A set of ground-based observatories were designed, constructed and fielded as an integral part of the NASA THEMIS satellite program so that the substorm onsets could be timed and located. The instrumentation was designed to cover a large region of the northern arctic in the Canadian and Alaskan sectors. The instruments have a demonstrated high light sensitivity, permitting short exposure and high time resolution. They were designed to incur relatively modest construction costs. The stations were also designed to operate reliably in the Arctic, requiring minimum maintenance. Operation of the chain in the winter of 2005–06 and 2006–07 validated the station design concepts and produced data set that are scientifically useful in

their own right. An example of the data set taken during the substorm of December 23, 2006 was presented in this paper. In this example, the onset brightening took 27 seconds, which is too long for an effective time marker to satisfy the THEMIS timing requirements. However, the auroral arc breakup was relatively instantaneous and could be timed to the nearest 3-second, located to the nearest latitude degree and to about ± three degrees in longitude. During the initial arc brightening, the intensification of the magnetic field variations was also quite slow. The largest intensification took place after breakup. Significant magnetic impulses in the Pi2 frequency range occurred, but with a significant (∼40 s) delay. The long periods associated with these type pulsations limited their timing accuracy. In summary, the THEMIS GBOs satisfies the timing and location requirements dictated by the THEMIS program. The coordinated operation of the ground based observatories and the THEMIS satellites will create unprecedented opportunities to study auroral magnetospheric physics.

## References

S.-I. Akasofu, The dynamical morphology of the aurora polaris. J. Geophys. Res. **68**, 1667 (1963)

S.-I. Akasofu, The development of the auroral substorm. Planet. Space Sci. **12**, 273 (1964). doi:10.1016/0032-0633(64)90151-5

S.-I. Akasofu, Dynamic morphology of auroras. Space Sci. Rev. **4**, 498 (1965). doi:10.1007/BF00177092

S.-I. Akasofu, *Polar and Magnetospheric Substorms* (Reidel, Dordrecht, 1968)

S.-I. Akasofu, Magnetospheric substorms: A model, in *The Magnetosphere: Part III of Solar-terrestrial Physics/1970* (Reidel, Dordrecht, 1972), pp. 131–151

S.-I. Akasofu, *Physics of Magnetospheric Substorms* (Reidel, Dordrecht, 1977), p. 358

V. Angelopoulos, The THEMIS mission. Space Sci. Rev. (2008, this issue)

D.N. Baker, T.I. Pulkkinen, V. Angelopoulos, W. Baumjohann, R.L. McPherron, Neutral line model of substorms: past results and present view. J. Geophys. Res. **101**, 12975–13010 (1996)

J.W. Chamberlain, *Physics of the Aurora and Airglow*. International Geophysics Series (Academic Press, San Diego, 1961)

C.C. Chaston, L.M. Peticolas, C.W. Carlson, J.P. McFadden, F. Mozer, M. Wilber, G.K. Parks, A. Hull, R.E. Ergun, R.J. Strangeway, M. Andre, Y. Khotyaintsev, M.L. Goldstein, M. Acuña, E.J. Lund, H. Reme, I. Dandouras, A.N. Fazakerley, A. Balogh, Energy deposition by Alfvén waves into the dayside auroral oval: Cluster and FAST observations. J. Geophys. Res. **110**(A2), A02211 (2005)

T.N. Davis, The application of image orthicon techniques to auroral observation. Space Sci. Rev. **6**, 222 (1966)

E.F. Donovan, S. Trond, L.L.C. Trondsen, B.J. Jackel, All-sky imaging within the Canadian CANOPUS and NORSTAR. Sodankyla Geophys. Observatory Publ. **92**, 109–112 (2003)

E.F. Donovan, S. Mende, B. Jackel, H. Frey, M. Syrjäsuo, I. Voronkov, T. Trondsen, L. Peticolas, V. Angelopoulos, S. Harris, M. Greffen, M. Connors, The THEMIS all-sky imaging array—system design and initial results from the prototype imager. J. Atmos. Terr. Phys. **68**, 1472–1487 (2006)

L.A. Frank, J.D. Craven, K.L. Ackerson, M.R. English, R.H. Eather, R.L. Carovillano, Global auroral imaging instrumentation for the Dynamics Explorer mission. Space Sci. Instrum. **5**, 369–393 (1981)

L.A. Frank, J.D. Craven, Imaging results from Dynamics Explorer 1. Rev. Geophys. **26**, 249–283 (1988). doi:10.1029/RG026i002p00249

H.U. Frey, S.B. Mende, V. Angelopoulos, E.F. Donovan, Substorm onset observations by IMAGE-FUV. J. Geophys. Res. **109**, A10304 (2004). doi:10.1029/2004JA010607

S.E. Harris, S.B. Mende, V. Angelopoulos, W. Rachelson, E. Donovan, B. Jackel, M. Greffen, C.T. Russell, D.R. Pierce, D.J. Dearborn, K. Rowe, M. Connors, THEMIS, Ground based observatory system design. Space Sci. Rev. Online First (SSRv Homepage) (2007). doi:10.1007/s11214-007-9294-z

J.H. Hecht, D.J. Strickland, M.G. Conde, The application of ground-based optical techniques for inferring electron energy deposition and composition change during auroral precipitation events. J. Atmos. Solar-Terr. Phys. **68**(13), 1502–1519 (2006)

E.W. Hones Jr., Plasma sheet variations during substorms. Planet. Space Sci. **20**, 1409 (1972). doi:10.1016/0032-0633(72)90048-7

A.T.Y. Lui, A synthesis of magnetospheric substorm models. J. Geophys. Res. **96**, 1849–1856 (1991). doi:10.1029/90JA02430

D. Lummerzheim, J. Lilenstein, Electron transport and energy degradation in the ionnosphere: Evaluation of the numerical solution, comparison with laboratory experiments and auroral observations. Ann. Geophys. **12**, 1039–1051 (1994)

E. Maggs, T.N. Davis, Measurements of the thicknesses of auroral structures. Planet. Space Sci. **16**, 205 (1986)

R.L. McPherron, C.T. Russell, M.P. Aubry, Satellite studies of magnetospheric substorms on August 15, 1968. J. Geophys. Res. **78**, 3131–3149 (1973). doi:10.1029/JA078i016p03131

S.B. Mende, R.H. Eather, E.K. Aamodt, Instrument for the monochromatic observation of all-sky auroral images. Appl. Opt. **16**, 1691–1700 (1977)

S.B. Mende, H.U. Frey, S.P. Geller, J.H. Doolittle, Multistation observations of auroras: Polar cap substorms. J. Geophys. Res. **104**, 2333–2342 (1999). doi:10.1029/1998JA900084

S.B. Mende, H. Heetderks, H.U. Frey, M. Lampton, S.P. Geller, S. Habraken et al., Far ultraviolet imaging from the IMAGE spacecraft. 1. System design. Space Sci. Rev. **91**, 243–270 (2000). doi:10.1023/A:1005271728567

S.B. Mende, C.W. Carlson, H.U. Frey, L.M. Peticolas, N. Østgaard, FAST and IMAGE-FUV observations of a substorm onset. J. Geophys. Res. **108**, 1344 (2003). doi:10.1029/2002JA009787

S.B. Mende, V. Angelopoulos, H.U. Frey, S. Harris, E. Donovan, B. Jackel et al., Determination of substorm onset timing and location using the THEMIS ground based observatories. Geophys. Res. Lett. **34**, L17108 (2007). doi:10.1029/2007GL030850

J.L. Posch, M.J. Engebretson, S.B. Mende, H.U. Frey, R.L. Arnoldy, M.R. Lessard, A comparison of Antarctic Pi1 signatures and substorm onsets recorded by the WIC imager on the IMAGE satellite. American Geophysical Union, Spring Meeting 2004, abstract #SM53B-05 (2004)

T.J. Rosenberg, Recent results from correlative ionosphere and magnetosphere studies incorporating antarctic observations. Adv. Space Res. **25**(7–8), 1357–1366 (2000)

M.T. Syrjäsuo, T.I. Pulkkinen, P. Janhunen, A. Viljanen, R.J. Pellinen, K. Kauristie, S. Wallman, P. Eglitis, P. Karlsson, O. Amm, E. Nielsen, C. Thomas et al., Observations of substorm electrodynamics using the MIRACLE network, in *Proceedings of the ICS-4* (2002)

M.R. Torr, D.G. Torr, M. Zukic, R.B. Johnson, J. Ajello, P. Banks et al., A far ultraviolet imager for the international solar-terrestrial physics mission. Space Sci. Rev. **71**, 329–383 (1995). doi:10.1007/BF00751335